Explore Stochastic Instabilities of Periodic Points by Transition Path Theory

Yu Cao, Ling Lin & Xiang Zhou

Journal of Nonlinear Science

ISSN 0938-8974
Volume 26
Number 3

J Nonlinear Sci (2016) 26:755-786
DOI 10.1007/s00332-016-9289-6

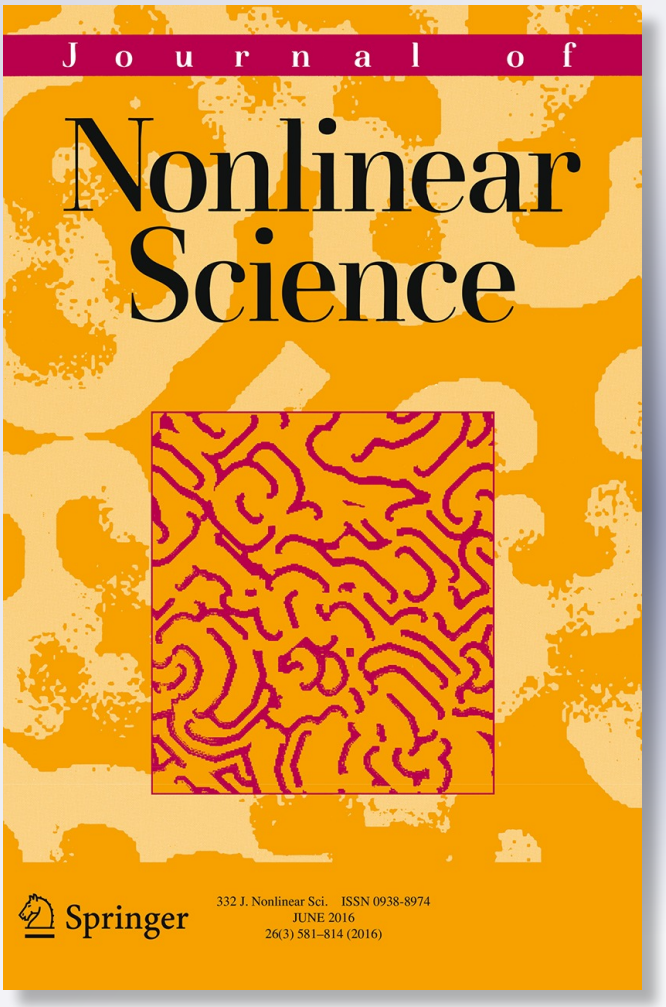

Springer

J Nonlinear Sci (2016) 26:755–786
DOI 10.1007/s00332-016-9289-6

Journal of Nonlinear Science

Explore Stochastic Instabilities of Periodic Points by Transition Path Theory

Yu Cao[1] · **Ling Lin**[2] · **Xiang Zhou**[1]

Received: 6 May 2015 / Accepted: 5 February 2016 / Published online: 18 March 2016

Abstract We consider the noise-induced transitions from a linearly stable periodic orbit consisting of T periodic points in randomly perturbed discrete logistic map. Traditional large deviation theory and asymptotic analysis at small noise limit cannot distinguish the quantitative difference in noise-induced stochastic instabilities among the T periodic points. To attack this problem, we generalize the transition path theory to the discrete-time continuous-space stochastic process. In our first criterion to quantify the relative instability among T periodic points, we use the distribution of the last passage location related to the transitions from the whole periodic orbit to a prescribed disjoint set. This distribution is related to individual contributions to the transition rate from each periodic points. The second criterion is based on the competency of the transition paths associated with each periodic point. Both criteria utilize the reactive probability current in the transition path theory. Our numerical results for the logistic map reveal the transition mechanism of escaping from the stable periodic orbit and identify which periodic point is more prone to lose stability so as to make successful transitions under random perturbations.

Communicated by Paul Newton.

Ling Lin acknowledges the financial support of the DRS Fellowship Program of Freie Universität Berlin. Xiang Zhou acknowledges the financial support of Hong Kong GRF (109113, 11304314, 11304715).

✉ Xiang Zhou
xiang.zhou@cityu.edu.hk

[1] Department of Mathematics, City University of Hong Kong, Tat Chee Ave, Kowloon, Hong Kong SAR

[2] Institute for Mathematics, Freie Universität Berlin, Arnimallee 6, 14195 Berlin, Germany

Keywords Random logistic map · Transition path theory · Periodic orbit · Stochastic instability

1 Introduction

For randomly perturbed dynamic systems, it is well known that regardless how small the noise amplitude is, the stochastic perturbation may have a significant influence on the long timescale. For example, thermal noise can induce important physical and biological metastability phenomena such as phase transitions, nucleation events and conformational changes in macromolecules. These phenomena correspond to very unlikely excursions of the random trajectories in the phase space, so these events are usually called *rare events*. The trajectories have to overcome some barriers to escape from the initial metastable state in order to enter another. To understand the occurrence of rare events, it is of great importance to investigate the nonequilibrium statistical and dynamic behaviors of those trajectories making successful transitions. Some interesting questions concern how the ensemble of these successful trajectories depend on the phase space of the unperturbed deterministic dynamic system: For example, what structures in the phase space would be the dynamical bottlenecks responsible for transition barriers; how the system leaves the initial metastable state and escapes its accompanying basin of attraction, etc. For general dynamics, the metastable state may not be a single point such as a local minimum on potential energy surface; it may be a collection of points, such as limit cycle, periodic orbit, or even chaotic attractor. In this paper, we are interested in determining through which location *inside* the metastable set the transition trajectories will leave with a higher or dominant probability. As a concrete example, we focus on stable periodic orbits in the randomly perturbed logistic map.

In history, a vast majority of research aims to explore the barrier on the basin boundary. For the diffusion process on a potential energy surface (a classic model for chemical reactions Karmers 1940; Kampen 1992), the well-known transition-state theory (Eyring 1935) states that the transition state is a saddle point with index 1 on the potential energy surface. The progress of chemical reactions is mainly described by "minimum energy paths", which are the heteroclinic orbits connecting two local minima through intervening saddle points. One can also calculate the transition rate by computing the probability flux of particles that cross the dividing surface of two neighboring potential wells. The concept of "most probable path" is very useful to describe transitions under random perturbations for general continuous-time dynamic systems. This path is a curve in the phase space with a dominant contribution to the likelihood of transition trajectories at vanishing noise limit. From the mathematical viewpoint, this most probable path is based on the large deviation principle (LDP) for the underlying stochastic system. For instance, the well-known Freidlin–Wentzell theory (Freidlin and Wentzell 1998) shows that the most probable transition path from a set A to another set B is the *minimum action path*, which minimizes the rate function of the Freidlin–Wentzell LDP (also known as "Freidlin–Wentzell action functional") subject to the boundary value condition starting from A and ending inside B. The transition probability is dominantly determined by the minimal value of the rate function.

Therefore, by analytically performing asymptotic analysis such as WKB or instanton analysis (Matkowsky et al. 1983; Naeh et al. 1990; Maier and Stein 1992, 1993), or by numerically solving some variational problem in the path space (E et al. 2004; Zhou et al. 2008; Heymann and Vanden-Eijnden 2008), one can identify the most probable escape/transition path. This allows a close examination of the path and unstable structures in the phase space. This idea based on the least action principle is quite applicable for general continuous- or discrete-time dynamic systems. Applications to the Lorenz model (Zhou 2009) and the Kuramoto–Sivashinsky PDE (Wan et al. 2010) have already discovered the barriers on the basin boundary in types of saddle points or saddle cycles.

For discrete maps perturbed by noise, there have also been extensive investigations on the effect of random perturbations. Some works are based on brute-force simulation to collect the empirical distributions of transition trajectories (Dykman et al. 1992). Applications of the large deviation rate function in the setting of discrete-time maps have appeared quite early in Kautz (1987, 1988). The authors studied the transitions between stable fixed points, stable periodic orbits and chaotic attractors and also showed empirical evidence that some transition state is saddle node. The research in Graham et al. (1991), Kraut and Feudel (2003) used the *quasi-potential* (activation energy) as a quantification of the stochastic stability for a metastable set and investigated certain key invariant set on the basin boundary. The series work of Luchinsky and Khonanov (1999), Silchenko et al. (2003, 2005) carried extensive computations for the Lorenz model, Henon map and other discrete-time maps under additive random perturbations. Their results seem to suggest that in the noise-induced escape from the basin of attraction of a stable invariant set, the barrier crossing on the basin boundary is mostly determined by the position and stability properties of certain saddle points or saddle cycles. Recently, a new approach has been developed in Billings et al. (2002), Bollt et al. (2002) to understand transport in stochastic dynamic systems. They use the transition probability matrix (after discretizing and reindexing the continuous space) to identify active regions of stochastic transport. Most of these existing studies deal with the transition state (or the set) on the basin of attraction of a metastable state (or invariant set).

In this paper, we are interested in the transitions from set to set with the purpose of pinpointing the role of individual points in the initial metastable set. The motivation comes from the questions: How the randomly perturbed system leaves the periodic orbit (or limit cycle in continuous-time dynamics); how the stable self-sustained oscillating motion eventually destroyed by the noise.

Specifically, we consider the random logistic map with additive Gaussian noise. We are concerned with the noise-induced transitions from A to B—two disjoint sets in the phase space. It is assumed that the unperturbed system has a linearly stable periodic orbit (all eigenvalues are less than one in modulus), denoted as $\boldsymbol{\xi} = (\xi_1, \xi_2, \ldots, \xi_T)$, where integer T is the period. To explore the stochastic instability of $\boldsymbol{\xi}$, we select A as the union of the T periodic points $\{\xi_i\}$ (more precisely, A is the union of T small windows around $\{\xi_i\}$. Refer to the full details in Sect. 2). Due to the noise, the stochastic system will eventually get a chance to make a significant transition to a distant set B away from A, after an exponentially long time wandering around the metastable set A in random motions of nearly periodic oscillation. The question we

shall address is how the system deviates from typical periodic oscillations, and when the deviation does happen, whether the perturbed system has any preference to some special periodic point to make the final successful transition toward B.

Traditional techniques based on the large deviation principle and the concept of quasi-potential are not capable of addressing the above questions, although they study the most active regions on the basin boundary of set A. If the unperturbed deterministic flow can go from a point x to another point y, then the cost (quasi-potential) from x to y is simply zero. Thus, if any two points in set A can reach each other by the deterministic flow (periodic orbit or limit cycle certainly satisfies this condition), then the quasi-potential is entirely flat on the whole set A. This means from any point in A, the minimal action to escape the basin is the same. The extremal path minimizing the action functional will take infinite time and usually also has an infinite length, and the whole set A is the α-limit set of the extremal path. This suggests that there is no particular location in the invariant set A from which the extremal path emits. The action functional and the minimum action path cannot distinguish individual points inside A in such cases. Similarly, the singular perturbation method (Matkowsky and Schuss 1982) for the mean first passage time in the vanishing noise limit will give a constant value of the WKB solution on the stable limit cycle and thus may not be useful to our problem unless the prefactor is included.

Here we use a new and attractive tool, the transition path theory (E and Vanden-Eijnden 2006, 2010; Vanden-Eijnden 2006; Metzner et al. 2009). The transition path theory for continuous-time dynamical systems has been proved to be an effective mathematical tool to reveal transition mechanisms of a few complex physical and biological systems (Noé et al. 2009; Cameron and Vanden-Eijnden 2014). This article intends to use the transition path theory to study stochastic instability for random discrete maps. We shall formulate the transition path theory for the discrete-time continuous-space Markov process. We then use three key ingredients in the transition path theory, i.e., reactive current, transition rate and dominant transition path, to understand the escape mechanism from the periodic orbit A for any finite (nonvanishing) noise. To quantitatively compare the stochastic instability of the T individual periodic points, we propose two rules: The first is the distribution of the last passage position among these T points, and the second is the initial point of the dominant transition path. Numerical results obtained clearly show the applicability of this theory in quantitative understanding of the different roles of the individual points belonging to the same periodic orbit.

The paper is organized as follows. In Sect. 2, we will set up our problem for the random logistic map. In Sect. 3, we briefly review the existing methodologies. In Sect. 4, we present our method based on the transition path theory. In Sect. 5, we show numerical results for the random logistic map. Section 6 is our concluding discussion.

2 Random Logistic Map

The randomly perturbed discrete map of our interest is the following

$$x_{n+1} = F(x_n) + \sigma \eta_n$$

where $\eta_n \sim N(0,1)$ are *i.i.d.* standard normal random variables and the constant $\sigma > 0$ is the noise amplitude. In this paper, we focus on a well-known example of F: the logistic map. The logistic map is probably the simplest nonlinear mapping showing periodic and chaotic behaviors. It is popularly used as a discrete-time demographic model to represent population with density-dependent mortality. Mathematically, the logistic map is written

$$x \to F(x) := \alpha x(1-x),$$

where x is a number between zero and one that represents the ratio of existing population to the maximum possible population. $\alpha > 0$ is the parameter. When x is out of the interval $[0,1]$, the logistic map simply diverges to infinity and never returns. The dynamics of interest is in the interval $[0,1]$. There are two fixed points in this interval: 0 and $1-\frac{1}{\alpha}$. When $0 < \alpha < 1$, the point 0 is the only stable fixed point, and when $1 < \alpha < 3$, $1-\frac{1}{\alpha}$ is the only stable fixed point. Both fixed points become unstable for α larger than 3. $\alpha = 3$ is the parameter for the onset of a stable period-2 orbit, and this period-2 orbit disappears at $\alpha = 1+\sqrt{6} \approx 3.4495$, from which the period-4 orbit takes over. The stable period-2^n orbit is followed by the stable period-2^{n+1} orbit if α increases. This phenomenon is termed period-doubling cascade and leads to the onset of chaos. Apart from this, tangent bifurcation is found, e.g., the onset of stable period-3 orbit arises at $\alpha = 1+2\sqrt{2} \approx 3.828$. Further details about the logistic map can be found in some classic literature, e.g., Ott (1993).

The random logistic map of our interest is the following stochastic dynamics restricted on the interval $D = [0,1]$,

$$x_{n+1} = F(x_n) + \sigma\eta_n \mod 1\,, \tag{2.1}$$

where $F(x) = \alpha x(1-x)$. We here impose the periodic boundary condition for the Markov process $\{x_n\}$ so that all dynamics is restricted on the compact set D. This will guarantee the unique existence of the invariant measure and thus ergodicity holds for this stochastic process, which is a fundamental assumption in the transition path theory. Other type of boundary condition is also feasible such as the reflection boundary condition at $x = 0$ and $x = 1$.

The transition probability density of the discrete-time continuous-space Markov process (2.1) is

$$P(x,y) = \sum_{l\in\mathbb{Z}} \frac{1}{\sqrt{2\pi\sigma^2}} \exp\left(-\frac{1}{2\sigma^2}(y - F(x) + l)^2\right), \tag{2.2}$$

where the sum over the integer l is merely an adjustment for the periodic boundary condition we used here. The density of the unique invariant measure, $\pi(x)$, is the solution of the following balance equation

$$\int_D P(y,x)\pi(y)\,\mathrm{d}y = \pi(x). \tag{2.3}$$

In other words, $\pi(x)$ is the eigenfunction for the principle eigenvalue of the adjoint transition kernel.

Now, we specify the sets involved in the transition problems for the randomly perturbed logistic map (2.1). We restrict the study to linearly stable periodic orbit in this paper, so the parameter α will always be selected such that the only stable invariant set in the (unperturbed) logistic map is a (linearly) stable period-T orbit, denoted as $\boldsymbol{\xi} = (\xi_1, \xi_2, \ldots, \xi_T)$. The order of (ξ_i) in $\boldsymbol{\xi}$ is specified so that $\xi_{i+1} = F(\xi_i)$. We choose a small neighborhood A around the T periodic points. A disjoint set B will be specified later. With these setups, the noise-induced transitions from A to B, named as A–B transitions, will be our focus. The set A, as the union of the T disjoint small windows, is specified by a width δ_a as follows

$$A = \bigcup_{1\le i\le T} [\xi_i - \delta_a, \xi_i + \delta_a]. \tag{2.4}$$

It is possible to specify different widths for different periodic points, or set the subintervals asymmetric around ξ_i. It is also possible to use the level set of the invariant measure, $\{x : \pi(x) < \delta\}$, around the periodic points. Here we use (2.4) for simplicity. The set B is placed near the unstable fixed point 0 (or 1) with a width δ_b:

$$B = [0, \delta_b] \cup [1 - \delta_b, 1]. \tag{2.5}$$

δ_a and δ_b are small enough so that $A \cap B = \emptyset$ and $[\xi_i - \delta_a, \xi_i + \delta_a] \cap [\xi_j - \delta_a, \xi_j + \delta_a] = \emptyset$ for any $1 \le i < j \le T$. The set B in our logistic map example is around the unstable point, the "furthest" boundary point from the stable set A. In general situations, this set B is placed just outside the basin of attraction of the periodic orbit $\boldsymbol{\xi}$ and the instability result about $\boldsymbol{\xi}$ is typically robust for small noise amplitude.

We introduced the nonzero width δ_a for the periodic orbit $\boldsymbol{\xi}$ because the space is continuous, not discrete: At a fixed noise amplitude $\sigma > 0$, it makes no sense to consider stochastic trajectories exactly leaving or entering some singleton points. In practice, the specification of the window width δ_a should be given by the user who decides to what extent the system is deemed out of the oscillatory status.

Usually, the width δ_a should be small enough so that each set A_i can represent the transition behavior for point ξ_i inside. In theory, for a set A to truly reflect the transition mechanism of escaping from $\boldsymbol{\xi}$, the width δ_a should approach zero. In fact, all calculations are based on a finite δ_a. Since set A has the metastability property (linearly stable), then it follows that the conclusions based on the study of set A for finitely small δ_a are quite robust and indeed give correct insights about the transition mechanisms and stochastic instabilities for the stable periodic orbit $\boldsymbol{\xi}$.

3 Related Works

We first briefly review two existing methods for the study of stochastic systems. The known applications of both methods are mainly for exploring the basin boundary.

3.1 Large Deviation Principle

We give a glimpse of the large deviation principle (LDP) for randomly perturbed discrete map. For continuous-time diffusions processes, refer to the Freidlin–Wentzell theory in Freidlin and Wentzell (1998). We start from the transition probability for the random mapping $x_{n+1} = F(x_n) + \sigma\eta_n$, which is

$$p(x, y) = \frac{1}{\sqrt{2\pi\sigma^2}} \exp\left(-\frac{(y - F(x))^2}{2\sigma^2}\right).$$

With the fixed initial point x_0 at time 0 and ending point x_n at time n, the probability of a path $\boldsymbol{\gamma} = (x_0, x_1, \ldots, x_{n-1}, x_n)$ is

$$P[\boldsymbol{\gamma}] = \prod_{i=0}^{n-1} p(x_i, x_{i+1}) \propto Z_\sigma^{-1} \exp\left(-\frac{1}{\sigma^2} S[x_0, \ldots, x_n]\right), \tag{3.1}$$

where Z_σ^{-1} is the prefactor and the cost function S has the form of

$$S[\boldsymbol{\gamma}] = S[x_0, \ldots, x_n] = \frac{1}{2}\sum_{i=0}^{n-1}(x_{i+1} - F(x_i))^2. \tag{3.2}$$

This cost function S is actually the *rate function* of the LDP at the vanishing noise limit $\sigma \downarrow 0$. By the Laplace's method, the path probability $P[\boldsymbol{\gamma}]$ is asymptotically dominated by $\exp\left(-\frac{1}{\sigma^2} S_{\min}\right)$, where $S_{\min} = \min_\gamma S[\boldsymbol{\gamma}]$. The *minimum action path* (MAP) $\boldsymbol{\gamma}^*$ is such that $S[\boldsymbol{\gamma}^*] = S_{\min}$. If this minimal action $S_{\min}$ is viewed as a function of the initial point x_0 and the ending point x_n for all possible n, then it is the so-called *quasi-potential*, which is quite useful for quantifying the stability of each basin against the random perturbation (Freidlin and Wentzell 1998; Kautz 1987; E et al. 2012). When the initial point x_0 is in a stable structure (such as fixed point, periodic orbit and chaotic attractor) of the phase space, and x_n is out of the basin of attraction of this stable structure, the MAP is usually called the *most probable escape path* (MPEP). The intersection part of the MPEP with the basin boundary is quite revealing in search of transition states or active regions for crossing the boundary.

One obvious feature of this least action method based on the LDP is that the cost is *zero* for a path from ξ_1 to ξ_2 if ξ_2 is exactly equal to $F(\xi_1)$. This means that starting from any point in the same period-T orbit, the minimal action is the same. Thus, one can not tell which point in the periodic orbit, limit cycle or even chaotic attractor is more prone to random perturbation, since they share the same value of the minimal action.

3.2 PDF Flux

To study the bi-stabilities in the stochastically perturbed dynamical systems, Bollt et al. (2002), Billings et al. (2002) proposed a method on the transport of probability

density function under the discrete map, in which the one-step transport is described by the Frobenius–Perron operator, i.e., the adjoint of the transition kernel $P(x, y)$. They investigated how an initial distribution is transported to a given region in the phase space under the action of this operator:

$$\rho(x) \to \mathcal{F}[\rho](x) := \int_D P(y, x)\rho(y)\,\mathrm{d}y.$$

Depending on the initial distribution, they call $\mathcal{F}[\rho]$ the *area flux* if ρ is uniform and call $\mathcal{F}[\rho]$ the *PDF flux* if ρ is the invariant measure π (Eq. (2.3)). For a given set $A \subset D$, the "mass flux into A" is defined as

$$\int_{x\in A}\left(\int_{y\in D\setminus A} P(y, x)\rho(y)\,\mathrm{d}y\right)\mathrm{d}x$$

and "mass flux out of A " (by switching A and its complement set $D \setminus A$) is defined as

$$\begin{aligned}\mathcal{F}_A^- &= \int_{x\in D\setminus A}\left(\int_{y\in A} P(y, x)\rho(y)\,\mathrm{d}y\right)\mathrm{d}x\\ &= \int_{y\in D\setminus A}\left(\int_{x\in A} P(x, y)\rho(x)\,\mathrm{d}x\right)\mathrm{d}y\\ &= \int_{x\in A}\rho(x)\left(\int_{y\in D\setminus A} P(x, y)\,\mathrm{d}y\right)\mathrm{d}x.\end{aligned} \tag{3.3}$$

The quantity $\rho(x)P(x, y)$ was used for x in one basin and y in another basin to investigate where a trajectory is most likely to escape the basin boundary. For a few applications (Billings et al. 2002), the saddle cycles on the basin boundary usually have the maximal flux across the boundary.

4 Transition Path Theory for Discrete Map

Now, we return to our problem of the randomly perturbed logistic map (2.1). We will first formulate the transition path theory for discrete map. Then, we identify the point in the orbit $\boldsymbol{\xi}$ with the highest probability mass of being the last passage position during the A–B transition, which is actually the point with the biggest contributions to the transition rate. To further study the development of the transition probability currents after emitting the set A, we will carry out the pathway analysis and target for the dominant transition paths. The precise definitions of these concepts will be explained soon.

We remark that the first approach based on the transition rate is relatively easy and quite universal for any situations. The second path-based approach needs a thorough exploration of connected paths based on network theory, and thus, it could have difficult situations that fail to compare stochastic instability in a quantitative way due to complexity of pathways. Our logistic map example does not run into this problem-dependent difficulty and shows a clean result. In addition, the two approaches may

also give two different conclusions since the viewpoints of interpreting and comparing the stochastic instabilities are different.

4.1 Transition Path Theory (TPT) for Randomly Perturbed Discrete Map

The original TPT was formulated for the continuous-time continuous-space Markov process (E and Vanden-Eijnden 2006, 2010; Vanden-Eijnden 2006). The TPT for the continuous-time discrete-space Markov process (jump process) was developed in Metzner et al. (2009), in which a detailed analysis for the pathways on the discrete space is of particular interest. Here we present the method of TPT in the setting of the discrete-time continuous-space Markov process.

The transition path theory does not consider the limit of vanishing noise. It assumes that the stochastic system is ergodic and has a unique invariant measure. The main focus of the TPT is the statistical behavior of the ensemble of *reactive trajectories* between two arbitrary disjoint sets. Assume that A and B are two disjoint closed subsets of the state space D ($D = [0, 1]$ for our example of the logistic map), each of which is the closure of a nonempty open set. The transition of our interest is from A to B. For a discrete-time homogeneous Markov process $\{X_n : n \in \mathbb{Z}\}$, define the first hitting time after time m and the last hitting time before time m of $A \cup B$ as follows, respectively,

$$\begin{aligned} H^+_{AB}(m) &:= \inf\{n \geq m : X_n \in A \cup B\}, \\ H^-_{AB}(m) &:= \sup\{n \leq m : X_n \in A \cup B\}. \end{aligned} \tag{4.1}$$

Then, for a generic trajectory $(X_n)_{n\in\mathbb{Z}}$, the ensemble of A–B **reactive trajectories** is defined the collection of pieces of the truncated trajectories: $\{X_n : n \in \mathsf{R}\}$, where $n \in \mathsf{R}$ if and only if

$$X_{H^+_{AB}(n+1)} \in B \quad \text{and} \quad X_{H^-_{AB}(n)} \in A.$$

R is the set of times which X_n belongs to an A–B reactive trajectory. Refer to Fig. 1 for one piece of reactive trajectory extracted from a generic trajectory. The intuition of A–B reactive trajectories is that the points on these reactive trajectories will first reach B rather than A and came from A rather than B.

The most important ingredient in the TPT is the probability current for A–B reactive trajectories. For the continuous state space D, we introduce its space-discretized version first:

$$\begin{aligned} \mathsf{J}(x, y, \Delta x, \Delta y) := \lim_{N\to\infty} \frac{1}{2N+1} \sum_{n=N}^{-N} \Bigg(& \mathbf{1}_{\left[x-\frac{\Delta x}{2}, x+\frac{\Delta x}{2}\right]}(X_n) \mathbf{1}_{\left[y-\frac{\Delta y}{2}, y+\frac{\Delta y}{2}\right]}(X_{n+1}) 0 \\ & \mathbf{1}_A\left(X_{H^-_{AB}(n)}\right) \mathbf{1}_B\left(X_{H^+_{AB}(n+1)}\right) \Bigg), \end{aligned} \tag{4.2}$$

where $\mathbf{1}_{\{\cdot\}}(\cdot)$ is the indicator function. The A–B **reactive probability current** is defined as the following limiting function for x and y in D,

$$J(x, y) := \lim_{\Delta x, \Delta y \to 0} \frac{\mathsf{J}(x, y, \Delta x, \Delta y)}{\Delta x \Delta y}.$$

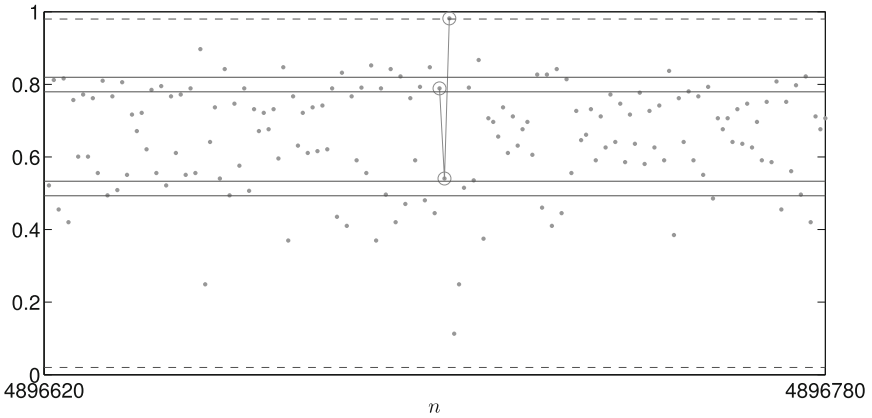

Fig. 1 The snapshot of a generic trajectory (dots in the plot) and one reactive trajectory (three points marked with circles) of the randomly perturbed logistic map observed in the time interval [4896620, 4896780]. The set A is the union of A_1 and A_2 around the periodic points $\boldsymbol{\xi} = (0.5130, 0.7995)$, corresponding to two narrow bands with length $2\delta_a = 0.04$ shown by *solid horizontal lines*. The bounds of the set B near 0 and 1 are shown by *dashed lines*. $\alpha = 3.2, \sigma = 0.04$

We sometimes just call J the reactive current whenever the specification of the sets A and B is clear.

The above definition of the reactive current J is based on the time average for an infinitely long generic trajectory. To obtain an ensemble average, we need to assume the Markov process $\{X_n\}$ is ergodic, i.e., the unique existence of the invariant probability density such that $\pi(x) = \lim_{N\to\infty} \frac{1}{N} \sum_{n=0}^{N-1} \mathbf{1}_{\{x\}}(X_n)$. Then, (4.2) leads to the following formula of the reactive current

$$J(x, y) = q^-(x)\pi(x)P(x, y)q^+(y), \quad x \in D, y \in D. \tag{4.3}$$

where $P(x, y)$ is the transition density function of the Markov process: $P(x, y)\,\mathrm{d}y = \mathbb{P}\left[X_{n+1} \in [y, y + \mathrm{d}y) | X_n = x\right]$. q^+ and q^- are called the forward and backward committor functions, defined as follows, respectively:

$$q^+(x) := \mathbb{P}[X_{H^+_{AB}(0)} \in B | X_0 = x], \quad q^-(x) := \mathbb{P}[X_{H^-_{AB}(0)} \in A | X_0 = x].$$

By definition, the committor functions satisfy the following boundary conditions

$$\begin{cases} q^+(x) = 0, \text{ and } q^-(x) = 1, & \text{if } x \in A, \\ q^+(x) = 1, \text{ and } q^-(x) = 0, & \text{if } x \in B. \end{cases} \tag{4.4}$$

This implies the fact

$$J(x, y) = 0, \quad \text{when } x \in B, y \in D \text{ or } x \in D, y \in A. \tag{4.5}$$

It is known from E and Vanden-Eijnden (2006), Metzner et al. (2009) that the committor functions satisfy the following Fredholm integral equation on the domain $x \in D \backslash (A \cup B)$, respectively,

$$q^+(x) = \int_D P(x, y)q^+(y)\,\mathrm{d}y, \tag{4.6}$$

and

$$q^-(x) = \int_D P^-(x, y)q^-(y)\,\mathrm{d}y, \tag{4.7}$$

where

$$P^-(x, y) := \frac{1}{\pi(x)}P(y, x)\pi(y) \tag{4.8}$$

is the transition kernel of the time-reversed process $\{X_{-n}\}_{n\in\mathbb{Z}}$. Since the transition kernel P is irreducible in the ergodicity assumption, then the functions $q^+(x)$ and $q^-(x)$ are always strictly positive for any $x \notin A \cup B$.

Remark 1 Compared with the PDF flux $\pi(x)P(x, y)$ in Sect. 3.2, the A–B reactive current $J(x, y) = \pi(x)P(x, y)q^-(x)q^+(y)$ in the transition path theory includes the additional global information for the A–B transitions encoded by the committor functions. These two quantities are equal only when $x \in A$ and $y \in B$.

We shall address two main issues about the methods based on the TPT for application to the random perturbed discrete map. The first is the robust calculation of reactive current function $J(x, y)$; the second is how to use this reactive current function to analyze reaction pathways as well as the reaction rate. Based on these developments, we shall carry out the study for the roles of individual points in A and evaluate their stability in the context of A–B transitions.

We rewrite the Eqs. (4.7) and (4.8) by introducing $\tilde{q}^-(x) := \pi(x)q^-(x)$,

$$\tilde{q}^-(x) = \int_D P(y, x)\tilde{q}^-(y)\,\mathrm{d}y, \quad x \in D\backslash(A \cup B). \tag{4.9}$$

The boundary condition is $\tilde{q}^-(x) = \pi(x)$ for $x \in A$ and $\tilde{q}^+(x) = 0$ for $x \in B$. Eq. (4.9) has the same form as Eq. (4.6) if transposing the transition kernel P. There are two reasons for introducing $\tilde{q}^-$: (1) The reactive current J, rather than q^- itself, is of more interest in understanding the transition mechanism, and it is not necessary to calculate q^- in order to obtain J; (2) the numerical method to calculate q^- directly is instable when the noise intensity σ is too small. This problem can be resolved by calculating $\tilde{q}^-$ instead.

The system (4.9) and (4.6) together with the boundary condition (4.4) can be solved as a linear system after discretizing the spatial domain $D = [0, 1]$. $q^+(x)$ and $\tilde{q}^-(x)$ typically exhibit boundary layers or discontinuities at the boundaries of A and B. In our numerical discretization, the spatial mesh grid is adjusted in a moving mesh style to distribute more points near the boundaries by checking the derivatives $|\nabla q^+|$ and $|\nabla\tilde{q}^-|$ (refer to Zhou et al. 2008 for details).

Since

$$J(x, y) = q^-(x)\pi(x)P(x, y)q^+(y) = \tilde{q}^-(x)q^+(y)P(x, y), \tag{4.10}$$

then we can see from (4.6) and (4.9) that

$$\begin{aligned}\int_{y\in D} J(x,y)\mathrm{d}y &= q^-(x)\pi(x)\int_{y\in D} P(x,y)q^+(y)\,\mathrm{d}y\\ &= \tilde{q}^-(x))q^+(x), \quad \forall x\notin (A\cup B); \qquad (4.11)\\ \int_{x\in D} J(x,y)\,\mathrm{d}x &= q^+(y)\int_{x\in D} P(x,y)\tilde{q}^-(x)\,\mathrm{d}x\\ &= \tilde{q}^-(y)q^+(y), \quad \forall y\notin (A\cup B). \qquad (4.12)\end{aligned}$$

The above quantity on the right hand sides is actually the probability density of reactive trajectories:

$$\pi^{\mathsf{R}}(x) := q^-(x)\pi(x)q^+(x) = \tilde{q}^-(x)q^+(x), \quad \forall x\in D\backslash(A\cup B).$$

From the ergodicity condition, this probability density $\pi^{\mathsf{R}}(x)$ corresponds to the following time average: $\pi^{\mathsf{R}}(x)\,\mathrm{d}x = \lim_{N\to\infty}\frac{1}{2N+1}\sum_{-N}^{N}\mathbf{1}_{\mathsf{R}}(n)\mathbf{1}_{[x,x+\mathrm{d}x)}(X_n)$. Equations (4.11) and (4.12) together show that

$$\int_{y\in D} J(x,y)\,\mathrm{d}y = \int_{y\in D} J(y,x)\,\mathrm{d}y = \pi^{\mathsf{R}}(x), \quad \text{for any } x\in D\backslash(A\cup B). \qquad (4.13)$$

So, the reactive current $J(x,y)$ defines a flow at any $x\in D\backslash(A\cup B)$ since the inflow is equal to the outflow.

Remark 2 For the transition kernel $P(x,y)$ based on the discrete map, it is possible that $q^{\pm}(x)$ is continuous only in the open set $D\backslash(A\cup B)$. The one-sided limit from the open set $D\backslash(A\cup B)$ may not equal the boundary value at ∂A or ∂B (note that A and B are closed set and $\partial A\subset A$, $\partial B\subset B$). Thus, there may be a jump discontinuity $q^{\pm}(x)$ at $x\in\partial A\cup\partial B$. Refer to Fig. 3 in the next section for the example of logistic map. This means that $J(x,y)$ in (4.10) may also have the jump discontinuities whenever x or y crosses the boundaries at $\partial A\cup\partial B$.

4.2 Transition Rate and Most-Probable-Last-Passage Periodic Point

The reactive current J allows us to calculate how frequently the transition occurs from A to B, i.e., the transition rate. The **transition rate** is the average number of transitions from A to B per unit time, defined by

$$\kappa_{AB} := \lim_{N\to\infty}\frac{\#\{\text{transitions from } A \text{ to } B \text{ in } [-N,N]\}}{2N+1}.$$

With the definition of the set R, we can rewrite the above as

$$\kappa_{AB} = \lim_{N\to\infty}\frac{1}{2N+1}\sum_{-N}^{N}\mathbf{1}_A(X_n)\mathbf{1}_{D\backslash A}(X_{n+1})\mathbf{1}_{\mathsf{R}}(n).$$

Remark 3 When the set A is the union of disjoint compact subsets $A = \cup_{i=1}^{K} A_i$, then it is obvious that the A–B transition rate has the following decomposition

$$\kappa_{AB} = \sum_{i=1}^{K} \kappa_{A_i B} := \sum_{i=1}^{K} \lim_{N\to\infty} \frac{1}{2N+1} \sum_{-N}^{N} \mathbf{1}_{A_i}(X_n)\mathbf{1}_{D\setminus A}(X_{n+1})\mathbf{1}_{\mathsf{R}}(n),$$

where R still means the A–B transitions. Then, the ratio $\frac{\kappa_{A_i B}}{\kappa_{AB}}$ is exactly the probability that the reactive trajectory selects the subset A_i to leave the set A during its last stay in the set A.

Using ergodicity, the transition rate is calculated as follows

$$\begin{aligned}\kappa_{AB} &= \int_{x\in A}\int_{y\in D\setminus A} J(x,y)\,\mathrm{d}y\,\mathrm{d}x = \int_{x\in A}\int_{y\in D} J(x,y)\,\mathrm{d}y\,\mathrm{d}x \\ &= \int_{x\in A} q^-(x)\pi(x)\int_{y\in D} P(x,y)q^+(y)\,\mathrm{d}y\,\mathrm{d}x \\ &= \int_{x\in A} \pi(x)\int_{y\in D} P(x,y)q^+(y)\,\mathrm{d}y\,\mathrm{d}x,\end{aligned} \tag{4.14}$$

where the definition $J(x,y) = \pi(x)P(x,y)q^-(x)q^+(y)$ and the facts that $J(x,y) = 0$ for $y \in A$ and $q^-(x) = 1$ for $x \in A$ are applied.

From Eq. (4.13), it is clear that

$$\int_{x\in A\cup B}\int_{y\in D} J(x,y)\,\mathrm{d}y\,\mathrm{d}x = \int_{x\in A\cup B}\int_{y\in D} J(y,x)\,\mathrm{d}y\,\mathrm{d}x.$$

By Eq. (4.5), the above equality becomes

$$\int_{x\in A}\int_{y\in D} J(x,y)\,\mathrm{d}y\,\mathrm{d}x = \int_{x\in B}\int_{y\in D} J(y,x)\,\mathrm{d}y\,\mathrm{d}x.$$

Thus, there is an equivalent formula for the transition rate:

$$\kappa_{AB} = \int_{x\in B}\int_{y\in D} J(y,x)\,\mathrm{d}y\,\mathrm{d}x = \int_{y\in B}\int_{x\in D} J(x,y)\,\mathrm{d}x\,\mathrm{d}y. \tag{4.15}$$

The transition rate (4.14) is the total contribution of the reactive current out of A and into B. To distinguish the different points in A, where the reactive current J is initiated, we introduce the following two functions $r^-_{AB}(x)$ and $r^+_{AB}(y)$ to represent the local contribution of the reactive current to the reaction rate:

$$r^-_{AB}(x) := \int_{D\setminus A} J(x,y)\,\mathrm{d}y = \int_D J(x,y)\,\mathrm{d}y, \qquad \text{for } x \in A, \tag{4.16}$$

$$r^+_{AB}(y) := \int_{D\setminus B} J(x,y)\,\mathrm{d}x = \int_D J(x,y)\,\mathrm{d}x, \qquad \text{for } y \in B. \tag{4.17}$$

Note that like Eq. (4.14), $r^-_{AB}(x) = \pi(x)\int_{y\in D} P(x,y)q^+(y)\,\mathrm{d}y$, requiring only the forward committor function q^+.

It is easy to see that r^-_{AB} and r^+_{AB} defined in (4.16) and (4.17), after normalization, are known as the reactive exit and reactive entrance distributions in the transition path theory (Cameron and Vanden-Eijnden 2014; Lu and Nolen 2015). Indeed, based on Remark 3, the probability density function of the last passage position on A of a typical reactive trajectory is then given by $r^-_{AB}(x)/\kappa_{AB}$ (note $\int_A r^-_{AB}(x)\,\mathrm{d}x = \kappa_{AB}$). Similarly, the probability density function of the first entrance position on B of a typical reactive trajectory is then given by $r^+_{AB}(y)/\kappa_{AB}$. We then define the *most-probable-last-passage point* in A as

$$\hat{x} := \arg\max_{x\in A} \frac{r^-_{AB}(x)}{\kappa_{AB}} = \arg\max_{x\in A} r^-_{AB}(x), \tag{4.18}$$

and the *most-probable-first-hitting point* in B as

$$\hat{y} := \arg\max_{y\in B} \frac{r^+_{AB}(y)}{\kappa_{AB}} = \arg\max_{y\in B} r^+_{AB}(y). \tag{4.19}$$

Of our particular interest is the most-probable-last-passage point $\hat{x}$ in A. We can think of this point as the most A–B "reactive" point in the set A. In terms of instability due to the noisy perturbation, this point is the least stable one in the set A conditioned on the transitions from A to B.

For the problem of the periodic orbits $\boldsymbol{\xi}$ in the logistic map, the set A is defined as the union of the neighbors of the T periodic points $\xi_1,\ldots,\xi_T$, i.e., $A = \cup_{1\le i\le T}[\xi_i - \delta_a, \xi_i + \delta_a]$. Since δ_a is small, we can use

$$r^-_{AB}(i) := \frac{1}{2\delta_a}\int_{\xi_i-\delta_a}^{\xi_i+\delta_a} r^-_{AB}(x)\,\mathrm{d}x. \tag{4.20}$$

to represent the contributions to the total flux κ_{AB} from point ξ_i. We define the **most-probable-last-passage periodic point** (abbreviated to "MPLP") as point $\xi_{\hat{i}}$ having the maximal value $\{r^-_{AB}(i) : i = 1,\ldots,T\}$. This MPLP is the most unstable periodic point in the transition from periodic orbit $\boldsymbol{\xi} = (\xi_1,\ldots,\xi_T)$ to set B.

Remark 4 The transition rate κ_{AB} is the integration over $x \in A$ for the function

$$\pi(x)\int_{y\in D\setminus A} P(x,y)q^+(y)\,\mathrm{d}y\,\mathrm{d}x.$$

As mentioned in Remark 1, compared with the PDF flux defined in Eq. (3.3) (where $\rho = \pi$), the difference between these two formulations is that $q^+(y)$ is multiplied onto $P(x,y)$ here. The inclusion of this forward committor function indicates that in the transition path theory, the object in focus is the A–B reactive trajectories, which have to reach the target set B *before* returning to A. The trajectories counted in the PDF flux (3.3) is a much larger set containing those trajectories which fail to reach B

but return to A. For the same stochastic system, κ_{AB} is usually much smaller than the quantity $\mathcal{F}_A^-$ in Eq. (3.3) unless B is infinitely close to $D\setminus A$.

The definition of the above MPLP is associated with the integration of the reactive probability current $J(x, y)$ for y over the set $D\setminus A$. It does not take account what happens after the reactive current leaves A from point x. So, it is possible that, once the reactive current flows out of A from a single MPLP $\hat{x}$, the reactive current actually quickly diverges and spreads out. As a result, in measurement of competency of paths from A to B, different transition paths might carry significantly different values of reactive currents. We then need to find the dominant one among all the transition paths connecting A and B. If we can successfully identify this dominant path, its starting point in set A will indicate this point has strong stochastic instabilities among all periodic points. When the dominant transition paths are not unique due to the complexity of the problem, it is possible that the starting points of these dominant transition paths may lie in multiple subsets A_i if $A = \cup_{i=1}^{T} A_i$: This simply means that all these subsets (or the periodic points) are equally instable by this path-based criterion.

4.3 Competency and Maximum Competency Periodic Point

The analysis of pathways is built on the **effective reactive probability current** $J^+(x, y)$, which is defined by

$$J^+(x, y) := \max(J(x, y) - J(y, x), 0). \tag{4.21}$$

$J^+(x, y)$ is always nonnegative and represents the net reactive flux from x to y. We may rewrite

$$J^+(x, y) = \frac{J(x, y) - J(y, x) + |J(x, y) - J(y, x)|}{2}.$$

Using Eq. (4.13), we obtain

$$\int_{y\in D} J^+(x, y)\,\mathrm{d}y = \int_{y\in D} J^+(y, x)\,\mathrm{d}y, \quad \text{for any } x \in D\setminus(A \cup B).$$

When $y \in A$, $J(x, y) = 0$, and it follows that when $x \in A$, $J^+(x, y) = \max(J(x, y) - J(y, x), 0) = J(x, y)$. The rate formula (4.14) can also be written in terms of the effective current J^+:

$$\kappa_{AB} = \int_{x\in A, y\in D} J(x, y)\,\mathrm{d}x\,\mathrm{d}y = \int_{x\in A, y\in D} J^+(x, y)\,\mathrm{d}x\,\mathrm{d}y.$$

The effective current $J^+(x, y)$ naturally leads to a series of concepts about the transition paths. These concepts are well described for countable discrete space in Metzner et al. (2009). Indeed, in terms of the algorithms, we can divide the continuous

domain D into a large number of very fine intervals (much smaller than the widths δ_a and δ_b) and apply the discrete algorithms based on the graph theory described in Metzner et al. (2009). The theoretical formulation we give below is for a continuous-space domain, and we believe this formulation has its own interest. To represent the effective current J^+, we shall use a generic two-dimensional function $f(x, y)$, which is defined on $D \times D$ and associated with the given disjoint sets A and B. This function $f(x, y)$ is an analogue of the weight for an edge from one node x to another y in the graph theory. Clearly, f has to meet the properties that J^+ does. We assume that the triplet (A, B, f) for a compact state space D satisfies the following assumption.

Assumption 1 (1) The sets A and B are disjoint nonempty closed subsets of the state space D and $A \cup B \subsetneqq D$;
(2) $f(x, y)$ is always nonnegative for all $(x, y) \in D \times D$ and

$$f(x, y) = 0, \quad \text{if } x \in B, y \in D \text{ or } x \in D, y \in A.$$

(3) $f(x, x) = 0, \quad \text{for } x \in D.$
(4) For $x \in D \backslash (A \cup B)$,

$$\int_{y \in D} f(x, y)\, \mathrm{d}y = \int_{y \in D} f(y, x)\, \mathrm{d}y.$$

(5) $f(x, y)$ is bounded and piecewise continuous in $D \times D$.

Definition 1 Given two disjoint subsets A', B' in D and the triplet (A, B, f) satisfying Assumption 1, for any $n \in \mathbb{N}$, $\boldsymbol{\omega} = (\omega_0, \omega_1, \ldots, \omega_n) \in D \times \cdots \times D$ is called an A'–B' **transition path** associated with (A, B, f), if

(1) $\omega_0 \in A', \omega_n \in B'$;
(2) $f(\omega_i, \omega_{i+1}) > 0$ for $0 \le i \le n - 1$.

Note that property (2) in Assumption 1 implies that $\omega_i \notin (A \cup B)$ for all $1 \le i \le n-1$.

We actually use $A' = A$ (or $A' \subset A$) and $B' = B$ in most cases. Occasionally, we need a different set B' from B. The following definition of the path competency is from the graph theory.

Definition 2 We define the **competency** of a path $\boldsymbol{\omega} = (\omega_0, \omega_1, \ldots, \omega_n)$ as the minimal value of $f(\omega_i, \omega_{i+1})$ for all $0 \le i \le n - 1$, that is,

$$\mathsf{Cp}(\boldsymbol{\omega}) := \min_{0 \le i \le n-1} f(\omega_i, \omega_{i+1}).$$

Remark 5 The notion of "competency" defined above is referred to as capacity in the context of graph theory. However, the terminology "capacity" is also used and plays a significant role in the classical potential theory for stochastic systems which is closely related to the transition path theory. To avoid confusion, we use a different terminology "competency".

Property (2) in Definition 1 implies that the competency of any A'–B' transition path is always strictly positive.

Definition 3 With the same assumption in Definition 1, a subset $\mathcal{C}$ of the product space $D \times D$ is called A'–B' f-**connected**, if there exists at least one A'–B' transition path $\boldsymbol{\omega} = (\omega_0, \omega_1, \ldots, \omega_n)$ for some $n \geq 1$, associated with the triplet (A, B, f), such that every directed edge (ω_i, ω_{i+1}) belongs to $\mathcal{C}$ for $0 \leq i \leq n-1$.

The collection of all A–B transition paths with length n and all edges contained in set $\mathcal{C}$ is denoted by $\mathbb{G}_n(\mathcal{C})$. $\mathbb{G}(\mathcal{C}) := \cup_n \mathbb{G}_n(\mathcal{C})$.

We drop out the function f most time and simply say the set $\mathcal{C}$ is A'–B' connected. We are particularly interested in the special set $\mathcal{C}$ as the superlevel set of the function f.

Definition 4 With the same assumption in Definition 1, define the superlevel set of function f for any nonnegative real number z,

$$L_z := \{(x, y) \in D \times D : f(x, y) \geq z\}.$$

The A'–B' **competency** of the function f, denoted as $z^*(A', B')$, is defined as

$$z^*(A', B') := \sup\left\{z \geq 0 : L_z \text{ is } A'\text{-}B'\text{connected}\right\}. \tag{4.22}$$

$L_{z^*(A',B')}$ is call the **minimal** A'–B' **connected superlevel set** of f if the maximizer can be reached:

$$z^*(A', B') = \max\left\{z \geq 0 : L_z \text{ is } A'\text{-}B' \text{ connected}\right\}.$$

As a convention, when A' and B' are not specified, A' is A and B' is B by default and we simply say the competency of the function f, the minimal connected set and denote $z^*(A', B')$ as z^*.

Remark 6 The relation between Definitions 2 and 4 is that

$$z^*(A', B') = \sup\left\{\mathsf{Cp}(\boldsymbol{\omega}) : \boldsymbol{\omega} \text{ is an } A'\text{–}B' \text{ transition path}\right\}. \tag{4.23}$$

Indeed, if $\boldsymbol{\omega}$ is an A'–B' transition path, then L_z is A'–B' connected for $z \leq \mathsf{Cp}(\boldsymbol{\omega})$; conversely, if L_z is A'–B' connected, then any A'–B' transition path $\boldsymbol{\omega} = (\omega_0, \omega_1, \ldots, \omega_n)$ with edges contained in L_z must satisfy $f(\omega_i, \omega_{i+1}) \geq z$ for all $0 \leq i \leq n-1$, thus $\mathsf{Cp}(\boldsymbol{\omega}) \geq z$. In particular, all the A–B transition paths with edges in the minimal A–B connected superlevel set L_{z^*} must have the same competency z^* as the function f.

Definition 5 With the same assumption in Definition 1, let $z^*(A', B')$ be the A'–B' competency of f in Definition 4. If $L_{z^*(A',B')}$ is A'–B' f-connected, we then call all the A'–B' transition paths with edges in $L_{z^*(A',B')}$ the A'–B' **dominant transition paths**. The A–B dominant transition paths are simply called the dominant transition paths.

In our problem about the periodic orbit $\boldsymbol{\xi} = (\xi_i)_{i=1,\ldots,T}$, the set A is $\cup_{i=1}^{T} A_i$ where $A_i = [\xi_i - \delta_a, \xi_i + \delta_a]$. Note the following important fact from (4.23),

$$z^*(A, B) = \max_i z^*(A_i, B).$$

Therefore, we propose to make use of the competencies, $z^*(A_i, B)$ for $1 \le i \le T$, to compare the instability of each ξ_i. The point $\xi_{\hat{i}}$ such that $z^*(A_{\hat{i}}, B) = \max_i z^*(A_i, B)$ is defined as the **maximum competency periodic point** (MCPP). The interpretation of this MCPP is that there exists a transition path emitting from this MCPP (more precisely, its window $A_{\hat{i}}$) whose competency is larger than any transition path emitting from any other periodic point. Thus, this MCPP is deemed the most active (least stable) periodic point in the noise-induced transition from A to B. If this MCPP $\xi_{\hat{i}}$ is unique, then all the dominant transition paths will start from $A_{\hat{i}}$. In case that the maximizers are not unique, the competencies $z^*(A_i, B)$ in general still give a ranking in terms of stochastic instability for all periodic points $\boldsymbol{\xi} = (\xi_i)$.

In the community of graph algorithms and network optimization, the dominant transition path is called the widest path, also known as the bottleneck shortest path or the maximum capacity path. There are plenty of practical algorithms to find the widest path (Ahuja et al. 1993). In what follows, we discuss the identification of the A–B competency z^* and the dominant transition paths. The purpose here is not to present details of the practical implements for discrete state space, but to demonstrate the concepts and the related theoretical properties in the continuous space.

It is easily seen from (4.23) that $z^* > 0$. If $z > \sup_{D\times D} f$, then L_z is empty. So, the competency z^* of f satisfies $0 < z^* \le \sup_{D\times D} f < \infty$. The following properties are obvious: (1) If L_{z_1} is connected, then so is L_{z_2} for any $z_2 < z_1$; (2) L_z is connected for any $0 < z < z^*$; and (3) L_z is not connected for any $z > z^*$. So, one can use a binary search algorithm to compute the competency z^* of f within the interval $(0, \sup_{(x,y)\in D\times D} f(x, y)]$. The obtained numerical result for z^* is a tiny interval $[z_l^*, z_u^*]$ bracketing the true value z^*. To judge a given set L_z is A–B f-connected, we can use the following set-to-set map Φ_z to propagate the set A until reaching B if it is reachable. The map Φ_z provides a set-tracking algorithm to search the transition path from A to B, an analogue of the breadth-first search algorithm. The same procedure is used to test every A_i–B f-connection in order to identify $z^*(A_i, B)$. Actually, since $A = \cup A_i$, the set-tracking is performed in parallel for all A_i.

Definition 6 For any $z > 0$, we define the map Φ_z on the collection of all subsets of D by

$$\Phi_z(C) =: \bigcup_{x\in C} \{y : (x, y) \in L_z\}, \quad \forall C \subset D.$$

Denote the compound mapping by

$$\Phi_z^m(C) := \Phi_z\left(\Phi_z^{m-1}(C)\right)$$

and $\Phi_z^0(C) := C$.

Let

$$N(z) := \min\left\{n \geq 1 : \Phi_z^n(A) \cap B \neq \emptyset\right\}.$$

So, $N(z)$ is the minimal length of all A–B transition paths. $N(z) < \infty$ if and only if L_z is A–B connected.

To avoid the technicality and ease the presentation, we assume that L_{z^*} is A–B f-connected, i.e., z^* is the maximizer in (4.22). Numerically, we check for z slightly below the numerical value z_l^*, and if for all tested z's, they share exactly the same $N(z)$ and the set $\Phi_z^{N(z)}(A) \cap B$ converges as z approaches z_l^*, and then, it is reliable to use the obtained numerical value z_l^* as the competency of f defined in (4.22).

4.4 Dominant Transition Path and Dynamical Bottleneck

Calculating the A_i–B competency, $z^*(A_i, B)$, suffices for quantifying the stochastic instabilities of the periodic points. In the last part of this section, we further discuss some additional issues about finding the A–B dominant transition paths since such paths can give us more details and insights about transition mechanism, especially how the periodic points compete in winning the global competency z^*.

First, we define a pullback operation.

Definition 7 Given $z \leq z^*$ and $n \geq N(z)$, let

$$W_z^{n,n} := \Phi_z^n(A) \cap B,$$

if this set is nonempty. And for $0 \leq i < n$, define

$$W_z^{n,i} := \{x \in \Phi_z^i(A) : \Phi_z(\{x\}) \cap W_z^{n,i+1} \neq \emptyset\},$$

recursively.

For any $\boldsymbol{\omega} = (\omega_0, \omega_1, \ldots, \omega_n)$, define the canonical projection $\pi_i : \boldsymbol{\omega} \mapsto \omega_i$. Then, we have the following property about the above set $W_z^{n,i}$.

Proposition 1 *For any $z \in (0, z^*]$, $n \geq N(z)$, and $0 \leq i \leq n$, then*

$$W_z^{n,i} = \pi_i\left(\mathbb{G}_n(L_z)\right),$$

which is to say

(1) for any $\alpha \in W_z^{n,i}$, there exists a transition path $\boldsymbol{\omega} = (\omega_0, \omega_1, \ldots, \omega_n) \in \mathbb{G}_n(L_z)$ with length n and $\omega_i = \alpha$.
(2) for any $\boldsymbol{\omega} = (\omega_0, \omega_1, \ldots, \omega_n) \in \mathbb{G}_n(L_z)$, $\omega_i \in W_z^{n,i}$ for all $0 \leq i \leq n$.

Proof (1): Pick up an arbitrary α in $W_z^{n,i}$, let $\omega_i := \alpha$, then there exists a point, denoted as ω_{i+1}, in both $\Phi_z(\{\omega_i\})$ and $W_z^{n,i+1}$. Since $\omega_{i+1} \in W_z^{n,i+1}$, we can inductively

find $\omega_j \in W_z^{n,j} \cap \Phi_z(\{\omega_{j-1}\})$ for $i < j \le n$; in particular, $\omega_n \in W_z^{n,n} \subset B$. Meanwhile, since $\omega_i \in \Phi_z^i(A)$, then there exists an ω_{i-1} such that $\omega_{i-1} \in \Phi_z^{i-1}(A)$ and $\omega_i \in \Phi_z(\{\omega_{i-1}\})$. From $\omega_{i-1} \in \Phi_z^{i-1}(A)$, we similarly have $\omega_j \in \Phi_z^j(A)$ and $\omega_{j+1} \in \Phi_z(\{\omega_j\})$ for $0 \le j < i$; in particular, $\omega_0 \in \Phi_z^0(A) = A$. It turns out that $\boldsymbol{\omega} := (\omega_0, \ldots, \omega_i, \ldots, \omega_n)$ is the desired transition path.

(2): Let $\boldsymbol{\omega} = (\omega_0, \omega_1, \ldots, \omega_n)$ be a transition path in the set L_z. Then, $\omega_0 \in A = \Phi_z^0(A)$. Note that $f(\omega_i, \omega_{i+1}) \ge z$ for all $0 \le i < n$, then $\omega_{i+1} \in \Phi_z(\{\omega_i\})$. In particular, $\omega_1 \in \Phi_z(\{\omega_0\}) \subset \Phi_z^1(A)$, and inductively, we have $\omega_i \in \Phi_z^i(A)$ for $0 \le i \le n$. Since $\omega_n \in B$, we have $\omega_n \in W_z^{n,n}$. Then, by induction again, we obtain from the definition of $W_z^{n,i}$ that $\omega_i \in W_z^{n,i}$ for $0 \le i \le n$. □

Definition 8 A pair $(x, y) \in D \times D$ is called an A–B **dynamical bottleneck**, or **dynamical bottleneck** for abbreviation, if $f(x, y) = z^*$ and $(x, y) \in W_{z^*}^{n,i} \times W_{z^*}^{n,i+1}$ for some $n \ge N(z^*)$ and $0 \le i < n$.

Proposition 2 *(1) If (x, y) is a dynamical bottleneck, then there exists a dominant transition path $\boldsymbol{\omega} = (\omega_0, \ldots, \omega_n)$ in $\mathbb{G}(L_{z^*})$, such that $x = \omega_i$ and $y = \omega_{i+1}$ for some i $(0 \le i < n)$.*

(2) If for the given set A, B and the function f, the bottleneck is unique, and then, every dominant transition path contains the bottleneck as one of its edges.

Proof (1) From the proof of Proposition 1, we see that if $x \in W_{z^*}^{n,i}$, there must exist an A-$\{x\}$ transition path $(\omega_0, \omega_1, \ldots, \omega_i = x)$ with edges in L_{z^*}, and if $y \in W_{z^*}^{n,i+1}$, then there is a $\{y\}$-B transition path $(\omega_{i+1} = y, \omega_{i+2}, \ldots, \omega_n)$ with edges in L_{z^*}. Since $(x, y) \in L_{z^*}$, then putting together the above two pieces, we obtain $\boldsymbol{\omega} = (\omega_0, \omega_1, \ldots, \omega_i = x, \omega_{i+1} = y, \omega_{i+2}, \ldots, \omega_n)$, which is a dominant transition path.

(2) By Remark 6, for every dominant transition path $\boldsymbol{\omega} = (\omega_0, \omega_1, \ldots, \omega_n)$ in $\mathbb{G}(L_{z^*})$, we have $\mathsf{Cp}(\boldsymbol{\omega}) = \min_i f(\omega_i, \omega_{i+1}) = z^*$. Let $i^* = \arg\min_i f(\omega_i, \omega_{i+1})$, then $f(\omega_{i^*}, \omega_{i^*+1}) = z^*$. It follows from Proposition 1 that $\omega_{i^*} \in W_{z^*}^{n,i^*}$ and $\omega_{i^*+1} \in W_{z^*}^{n,i^*+1}$. Hence, $(\omega_{i^*}, \omega_{i^*+1})$ is a bottleneck by definition. Since the bottleneck is unique, $(\omega_{i^*}, \omega_{i^*+1})$ must be the bottleneck (x, y). □

If the A–B dynamical bottleneck is unique, denoted as $\mathbb{B}(A, B) = (\mathbb{B}^-(A, B), \mathbb{B}^+(A, B))$, then we can furthermore recursively investigate how the dominant transition paths leave the set A and reach the bottleneck $\mathbb{B}(A, B)$. For example, we can define the bottleneck $\mathbb{B}(A, \mathbb{B}^-(A, B))$ for the transition from A to $\mathbb{B}^-(A, B)$, i.e., take $\mathbb{B}^-(A, B)$ as B'. If this bottleneck is also unique, we can continue to trace the nested bottlenecks $\mathbb{B}(A, \mathbb{B}^-(A, \cdots))$ back to some point in the set A. The final point obtained in this recursive way in the set A is just the MCPP we defined earlier.

4.5 Comments on Two Criteria of MPLP and MCPP

It is normal that our two criteria in Sects. 4.2 and 4.3 can give rise to different results in describing the stochastic instabilities of the same periodic point. The first criterion of looking for MPLP is to compare the total outflow of the reactive current from a periodic

point. The second criterion of looking for MCPP is to compare the competency of the "pipelines" from a periodic point in transporting the reactive current to the destination B. In other words, the MPLP is for the collective behavior of all pipelines, while the MCPP is about where the pipeline having the widest bottleneck lies. So, it is quite reasonable that in certain cases, the total flow is huge but the competency of each individual pipeline is actually small, or *vice versa*.

5 Application to the Random Logistic Map

We are now in position to apply the above two TPT-based methods to the logistic map for the set A and B specified in Sect. 2. The first result is for a fixed value $\alpha = 3.2$, at which a stable period-2 orbit exists. We shall show the numeric values of the A–B reactive probability current J and the analysis of the MPLP, MCPP and dominant transition paths. Then, by changing various parameter α and the noise amplitude σ, we study how the results change. During the discussion, we also show some validation work for the consistency with direct simulation and the robustness with respect to δ_a and δ_b.

5.1 Results for the Period-2 Case

5.1.1 Basic Quantities

(1) invariant measure π: pick up $\alpha = 3.2$ as an example. The stable period-2 orbit in this case is $\boldsymbol{\xi} = (\xi_1, \xi_2) = (0.5130, 0.7995)$. The invariant measure π at $\sigma = 0.04$ is shown in Fig. 2a, where the two peaks correspond to the locations of ξ_1 and ξ_2. It is seen that $\pi(\xi_1) < \pi(\xi_2)$, which implies that the periodic point ξ_2 on the right has a higher equilibrium probability. The same result $\pi(\xi_1) < \pi(\xi_2)$ for the two periodic

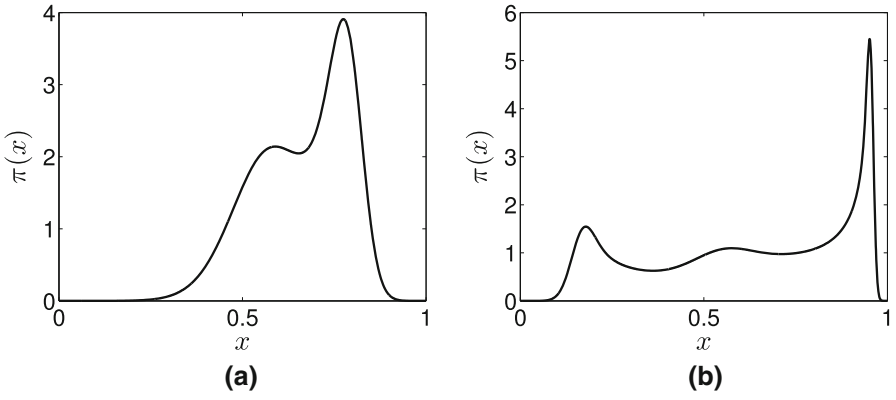

Fig. 2 The invariant probability density $\pi(x)$ for **a** the period-2 case and **b** the period-3 case. The parameters are **a** $\alpha = 3.2$, $\sigma = 0.04$, **b** $\alpha = 3.83$, $\sigma = 0.008$

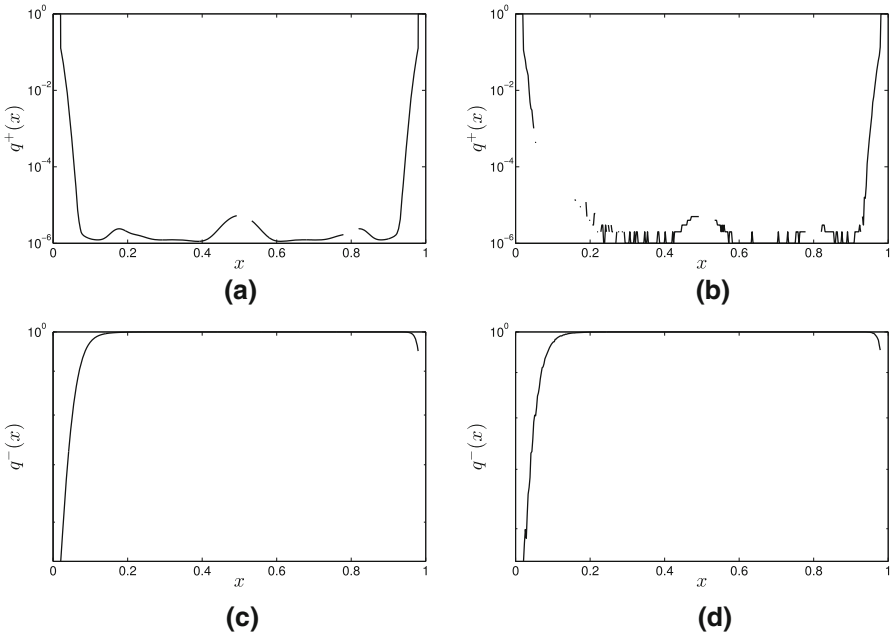

Fig. 3 The logarithmic plots of the forward committor function (**a**, **b**) and backward committor function (**c**, **d**). The parameters are $\alpha = 3.2$, $\sigma = 0.04$, $\delta_a = \delta_b = 0.02$. **a** $q^+(x)$ from solving (4.6), **b** $q^+(x)$ from direct simulation, **c** $q^-(x)$ from solving (4.7), **d** $q^-(x)$ from direct simulation

points $\xi_1 < \xi_2$ is observed for all values of α between [3.02, 3.40]. Actually, when α increases in this interval, the ratio $\pi(\xi_2)/\pi(\xi_1)$ also increases.

Figure 2b shows the invariant measure for a period-3 example at $\alpha = 3.83$. The period-3 orbit is $\boldsymbol{\xi} = (\xi_1, \xi_2, \xi_3) = (0.1561, 0.5047, 0.9574)$. To manifest the three peaks in the invariant measure for this periodic orbit, a smaller $\sigma = 0.008$ is used. It is clear here that the peak at $\xi_3 = 0.9574$ is dominantly large.

(2) Committor functions. Choose the sets A and B as specified in (2.4) and (2.5) with $\delta_a = \delta_b = 0.02$. The forward/backward committor functions q^+ and q^- at $\sigma = 0.04$ ($\alpha = 3.2$) are plotted in Fig. 3 at the logarithmic scale. The subplots (Fig. 3a, c) are the solutions obtained from the finite difference scheme for Eqs. (4.6) and (4.7) with a total 10000 mesh grid points. As a comparison, the same committor functions are calculated from the statistical average of a long trajectory by brute-force simulation of the random logistic mapping and they are shown in Fig. 3b, d. The total number of simulation time steps is 2×10^{10} (i.e., $N = 10^{10}$ in Eq. (4.14)), during which the number of successful transitions from A to B is 12238. Thus, the transition rate obtained from direct simulation is 6.119×10^{-7}. The transition rate calculated from the Eq. (4.14) is 6.008×10^{-7}.

It should be emphasized that the committor functions are not continuous at the boundary of the sets A and B. The forward committor function does not even change monotonically from 1 to 0. These special features come from the nature of the discrete-time map.

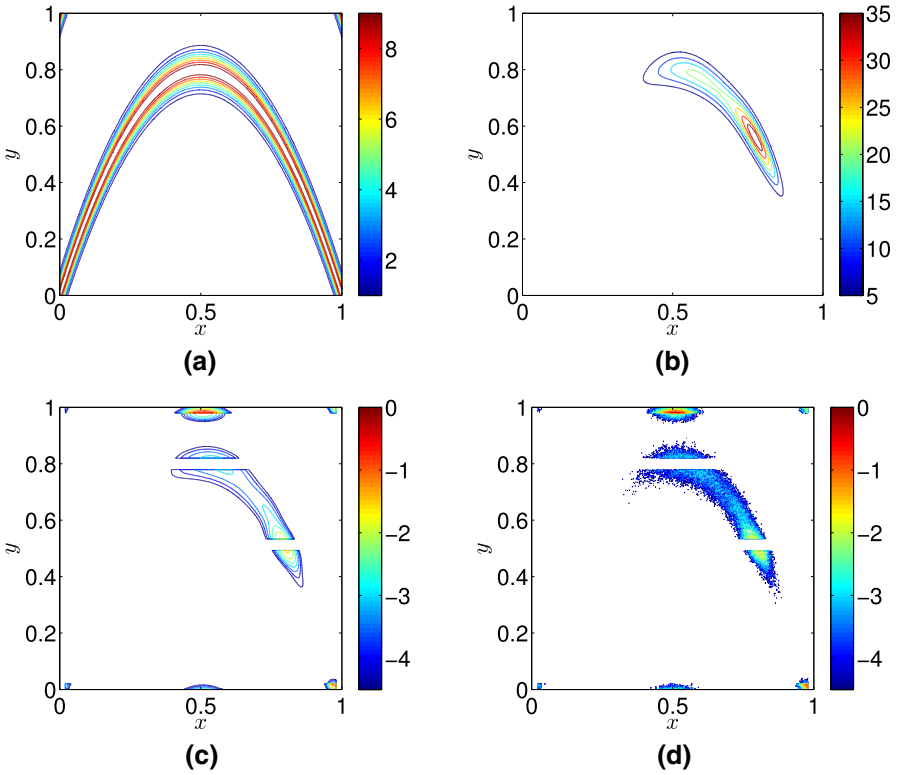

Fig. 4 The plots of the transition kernel $P(x, y)$, the PDF flux $\pi(x)P(x, y)$ used in Billings et al. (2002) and the A–B reactive current $J(x, y) = \pi(x)P(x, y)q^-(x)q^+(y)$. For better visualization, the contour plots for J in subplots (**c**) and (**d**) are actually for the value $\log(J(x, y)/M)$ where $M = \max_{x,y\in S} J(x, y)$. The parameters are $\alpha = 3.2$, $\sigma = 0.04$, $\delta_a = \delta_b = 0.02$. ($M = 6.5186 \times 10^{-4}$). **a** $P(x, y)$, **b** $\pi(x)P(x, y)$, **c** $J(x, y)$, **d** empirical $J(x, y)$

(3) A–B reactive current. Figure 4a shows the transition kernel $P(x, y)$. Figure 4b plots $\pi(x)P(x, y)$, which is the so-called PDF flux in Billings et al. (2002). The A–B reactive current in the TPT for our use, shown in Fig. 4c, was calculated from Eq. (4.10) via solving Eqs. (4.9) and (4.6) by using the finite difference method. Figure 4d is the empirical result from the direct simulation, which confirms that our calculation is reliable.

5.1.2 Comparison of Stochastic Instability at $\alpha = 3.08$

We fix $\sigma = 0.04$ for the following discussion about the transition mechanism at $\alpha = 3.08$. The period-2 orbit is $\boldsymbol{\xi} = (\xi_1, \xi_2) = (0.5696, 0.7551)$.

The first viewpoint, using MPLP, is to compare the total current out of $A : r^-_{AB}(x) = \int_D J(x, y)\,\mathrm{d}y$ for $x \in A$. The set A of concern is the union $A_1 \cup A_2$, where $A_i = [\xi_i - \delta_a, \xi_i + \delta_a]$, $i = 1, 2$. The set $B = [0, \delta_b] \cup [1 - \delta_b, 1]$. Table 1 shows that δ_a, the width of the set A, has little influence on the result of the transition rate κ_{AB}, and δ_b

Table 1 Transition rate k_{AB} for different δ_a and δ_b

k_{AB}	$\delta_a = 0.01$	$\delta_a = 0.015$
$\delta_b = 0.01$	4.6883×10^{-9}	4.6883×10^{-9}
$\delta_b = 0.015$	7.6215×10^{-9}	7.6215×10^{-9}

Here, $\alpha = 3.08$, $\sigma = 0.04$

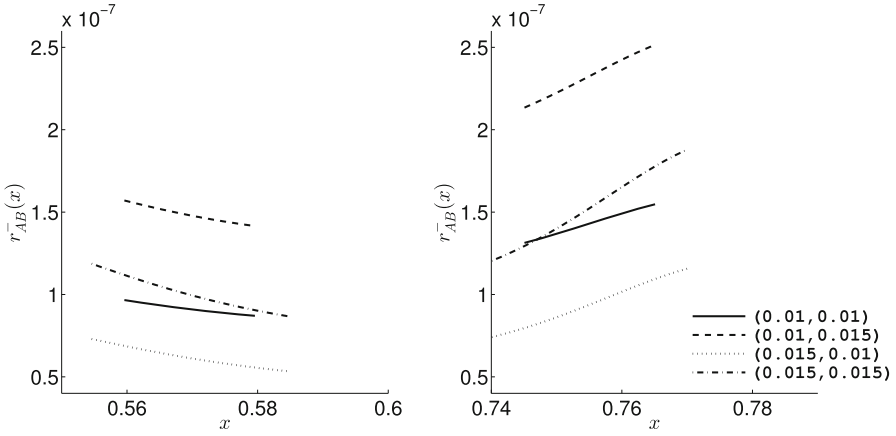

Fig. 5 $r^-_{AB}(x)$ for x in the union of the sets $A_1 = [\xi_1 - \delta_a, \xi_1 + \delta_a]$ (*left*) and $A_2 = [\xi_2 - \delta_a, \xi_2 + \delta_a]$ (*right*). $\boldsymbol{\xi} = (\xi_1, \xi_2) = (0.5696, 0.7551)$ is the period-2 orbit. $\alpha = 3.08$. $\sigma = 0.04$. The *solid lines* correspond to $\delta_a = 0.01, \delta_b = 0.01$; the *dashed lines* correspond to $\delta_a = 0.01, \delta_b = 0.015$; the *dotted lines* correspond to $\delta_a = 0.015, \delta_b = 0.01$; the *dash-dot lines* correspond to $\delta_a = 0.015, \delta_b = 0.015$

has a slightly more significant influence on κ_{AB}. This observation is expected since the set A is a small neighborhood of the linearly stable periodic orbit of the logistic map, while B not. To test the impact on the MPLP, we plot in Fig. 5 the total current $r^-_{AB}(x)$ for $x \in A_1$ (*left*) and $x \in A_2$ (*right*) for the different widths specified in Table 1. As this figure shows, the window A_2 containing the periodic point ξ_2 carries 30–50 % more reaction current than the window A_1, for various values of δ_a and δ_b. We also tested this result of the MPLP by varying σ between 0.01 and 0.04 and reached the same conclusion that the second periodic point ξ_2 is the MPLP.

So, our technique based on the relative size of the total current out of the set A robustly identifies the point ξ_2 from the period-2 orbit (ξ_1, ξ_2) as the MPLP. In the sense of the A–B transition events, we can claim that the point ξ_2 is less stable, or more active, under the random perturbation. Note that in terms of the invariant measure, $\pi(\xi_2) > \pi(\xi_1)$. It is ξ_1 that has a smaller equilibrium probability density.

In the following, we analyze the dynamical bottleneck and dominant transition pathways for this period-2 case. We will restrict to those dominant transition paths with the minimal path lengths $N(z^*)$ to exclude the possible existence of loops. For simplicity, we will omit $N(z^*)$ in the notation $W_{z^*}^{N(z^*),i}$ and write $W_{z^*}^i$. We choose the window width $\delta_a = \delta_b = 0.01$. After building the effective reactive current $J^+(x, y)$, we found that the A–B competency $z^* \approx 1.98 \times 10^{-6}$ by the binary search between 0 and $M = \max_{D\times D} J^+(x, y)$, and $N(z^*)$ is equal to 2. Then, we look for the sequences of the sets $W_{z^*}^i$ for $i = 2, 1, 0$, by using a number of pilot points to explore these sets. The numerical result, up to the accuracy of 10^{-4}, shows the following:

$$W^2_{z^*} = [0.9900, 0.9928] \subset B,$$
$$W^1_{z^*} = \{0.5331\} \subset D\backslash(A \cup B),$$
$$W^0_{z^*} = \{0.7651\} \subset A.$$

The A–B dynamical bottleneck $\mathbb{B}(A, B)$ is (0.7651, 0.5331). Let 0.5331 be the new set A' and search for the A'–B dynamical bottleneck. We obtain the second dynamical bottleneck (0.5331, 0.9900). Finally, we get the dominant transition path

$$\boldsymbol{\varphi} \approx (\underline{0.7651}, \underline{0.5331}, 0.9900), \quad \text{at} \quad \sigma = 0.04,$$

where the underlined values correspond to the positions of the dynamical bottlenecks. This result of dominant transition path is unchanged when we changed the mesh grid size between 1.7×10^{-4} and 3.4×10^{-4} in discretizing the space $D = [0, 1]$. We also varied the width δ_a between 0.01 and 0.02 and obtained the same result for the dominant transition path $\boldsymbol{\varphi}$. The first point of the dominant transition path $\boldsymbol{\varphi}$, i.e., the point in $W^0_{z^*}$, lies in the window A_2 for the second periodic point ξ_2. Thus, the A–B competency is actually realized by the A_2–B competency. So, we conclude that ξ_2 is the MCPP. The A–B dominant transition path starts from a boundary point in A_2, followed by a jump to some point on the left but far away from ξ_1 to escape the periodic orbit, and finally jumps into the set B.

5.2 Bifurcation Diagram for the Period-2 Case

It is interesting to see how the above transition mechanisms (MPLP, MCPP, dominant transition paths, etc.) change when the noise amplitude σ or the parameter α changes. The following numerical results show bifurcations for varying parameters, and we will see that the two criteria do not always give the same conclusion.

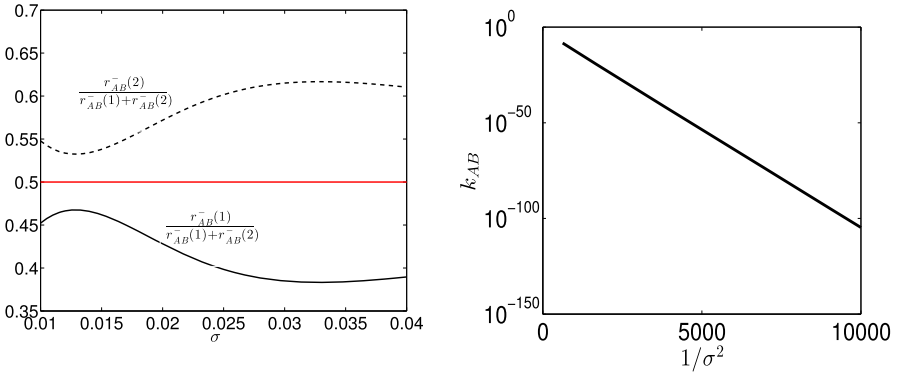

Fig. 6 **a** $\frac{r^-_{AB}(i)}{r^-_{AB}(1)+r^-_{AB}(2)}$ versus σ. **b** κ_{AB} versus $1/\sigma^2$

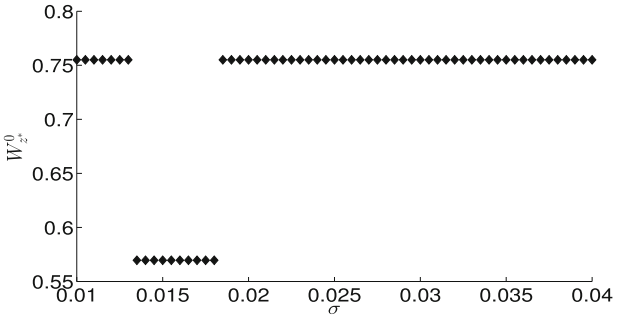

Fig. 7 The maximum competency periodic point

5.2.1 Change σ

We still fix $\alpha = 3.08$, but now change the value of the noise amplitude σ between 0.01 and 0.04. The period-2 orbit is $\boldsymbol{\xi} = (\xi_1, \xi_2) = (0.5696, 0.7551)$.

Figure 6a plots the probability density at ξ_1 and ξ_2 of the last hitting distribution of the transitions from A to B. It suggests that ξ_2 always wins ξ_1 as the MPLP for $\sigma \in (0.01, 0.04)$. The dependence of the transition rate κ_{AB} on the noise amplitude σ, in Fig. 6b, shows an Arrhenius-like relation.

From the results, the first observation is that the minimal length of the dominant transition paths, $N(z^*)$, grows as σ decreases. For example, at $\sigma = 0.02$, the dominant transition path is $\boldsymbol{\varphi} = (\underline{0.7651}, \underline{0.5269}, 0.9743, 0.0100)$. At $\sigma = 0.014$, the dominant transition path has minimal length 5:

$$\boldsymbol{\varphi} = (\underline{0.5596}, \underline{0.7761}, 0.5181, 0.9740, 0.0100).$$

At $\sigma = 0.013$, the dominant transition path has minimal length 6:

$$\boldsymbol{\varphi} = (0.7643, \underline{0.5508}, \underline{0.7818}, 0.5118, 0.9740, 0.0100).$$

When σ varies, the MCPP selected from the periodic points ξ_1 and ξ_2 is plotted in Fig. 7. This figure shows two critical values of σ : $\sigma_1 \approx 0.0134$ and $\sigma_2 \approx 0.0185$, where MCPP switches between ξ_1 and ξ_2.

We demonstrate a more detailed analysis at the bifurcation point σ_1 in Table 2 as well as in Fig. 8. Table 2 compares the A_i–B dominant transition paths $\boldsymbol{\varphi}_i$, $i = 1, 2$. That is $z^*(A_i, B) = \mathsf{Cp}(\boldsymbol{\varphi}_i)$ for $i = 1, 2$. The A–B dominant transition path $\boldsymbol{\varphi}$ is either $\boldsymbol{\varphi}_1$ or $\boldsymbol{\varphi}_2$, which has a larger competency. Keep in mind that the competency of a given path $(\varphi_0, \ldots, \varphi_N)$ is calculated as the minimum of the effective currents $J^+(\varphi_n, \varphi_{n+1})$ at each edge $(\varphi_n, \varphi_{n+1})$, which is highlighted in bold font in Table 2.

To understand the bifurcation of the MCPP, we need to analyze the competition of the two competencies $z^*(A_1, B)$ and $z^*(A_2, B)$, which are further determined by the A_i–B dynamical bottlenecks $\mathbb{B}(A_i, B)$ on the A_i–B dominant transition paths $\boldsymbol{\varphi}_i$ for $i = 1, 2$. The A_1–B dynamical bottleneck is the first step of jump on $\boldsymbol{\varphi}_1$: from the left boundary point of A_1 to a point (located at 0.77–0.78) near the right

Table 2 The A–B dominant transition path $\boldsymbol{\varphi}$ and the A–B competency z^* for three values of σ: $\sigma < \sigma_1$, $\sigma = \sigma_1$ and $\sigma > \sigma_1$

$\sigma =$	$0.0130 < \sigma_1$	$0.0134 \approx \sigma_1$	$0.0136 > \sigma_1$
$\boldsymbol{\varphi}_1 = (\xi_1, \cdots)$	0.5596, 0.7751, 0.5196, 0.9740, 0.0100	0.5596, 0.7758, 0.5186, 0.9740, 0.0100	0.5596, 0.7758, 0.5186, 0.9740, 0.0100
$J^+(\boldsymbol{\varphi}_1)$	**0.0150**, 0.0165, 0.0242, 0.3753	**0.0053**, 0.0063, 0.0093, 0.1255	**0.0243**, 0.0289, 0.0424, 0.5557
$\boldsymbol{\varphi}_2 = (\xi_2, \cdots)$	0.7644, 0.5509, 0.7818, 0.5119, 0.9740, 0.0100	0.7641, 0.5513, 0.7818, 0.5119, 0.9740 , 0.0100	0.7641, 0.5516, 0.7818, 0.5119, 0.9740, 0.0100
$J^+(\boldsymbol{\varphi}_2)$	0.0230, **0.0152**, 0.0260, 0.0363, 0.3753	0.0079, **0.0053**, 0.0091, 0.0126, 0.1255	0.0357, **0.0240**, 0.0410, 0.0567, 0.5557
$z^* =$	0.0152	0.0053	0.0243
$\boldsymbol{\varphi} =$	$\boldsymbol{\varphi}_2$	$\boldsymbol{\varphi}_1, \boldsymbol{\varphi}_2$	$\boldsymbol{\varphi}_1$

$\boldsymbol{\varphi}_1$ and $\boldsymbol{\varphi}_2$ are the A_1–B and A_2–B dominant transition paths, respectively. Their various dynamical bottlenecks are underlined. Their competencies are marked in bold font at the J^+ row (by multiplying the unit 10^{-58}, 10^{-54} and 10^{-53}, respectively, for each column). The A–B competency, z^*, is determined by the maximum of the A_1–B and A_2–B competencies. The periodic points $\boldsymbol{\xi} = (\xi_1, \xi_2)$ are located at $(0.5696, 0.7551)$ and $\delta_a = \delta_b = 0.01$

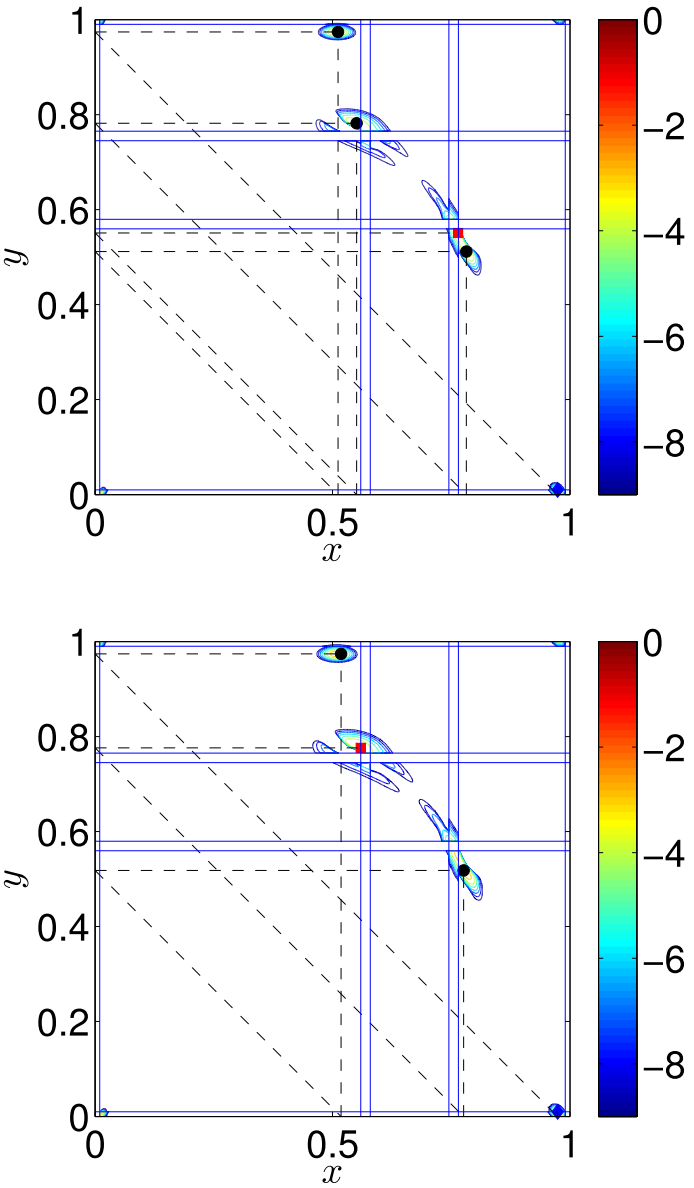

Fig. 8 This figure visualizes (in form of cobweb plot) the dominant transition path in the contour plot of $\log(J^+/M)$ where $M = \max_{x,y\in D} J^+(x,y)$ ($\alpha = 3.08, \delta_a = \delta_b = 0.01$). *Top* $\sigma = 0.013$; *Bottom* $\sigma = 0.014$. The six *vertical* and six *horizontal straight lines* (*solid*, *blue*) are the boundaries of A and B. The *red square-shaped dot* and *blue diamond-shaped dot* represent the first and the last edges of the path, respectively. The *black round dots* represent all the other edges

interval A_2. The A_2–B dynamical bottleneck is the second step in $\boldsymbol{\varphi}_2$: from a point slightly the left side of the interval A_1, to a point quite close to one point in the A_1–B dynamical bottleneck. For σ around the value σ_1, both of the A_i–B, $i = 1, 2$,

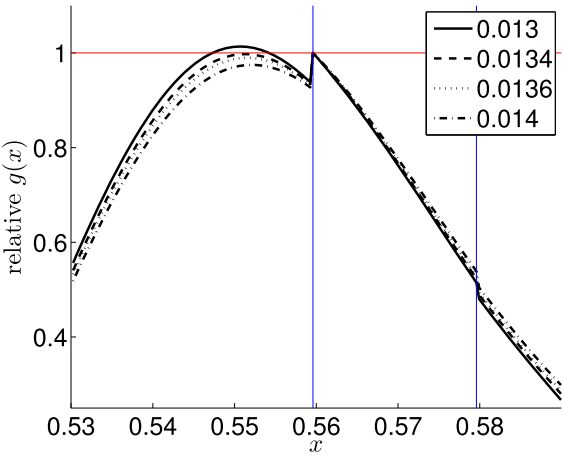

Fig. 9 The plot of $g(x)/g(\xi_1 - \delta_a)$ near A_1 for the four values of σ from 0.013 and 0.014. Note that g is not continuous at the boundary locations of A_1: $\xi_1 - \delta_a = 0.5596$ and $\xi_1 + \delta_a = 0.5796$, two *vertical lines* in this figure

dynamical bottlenecks are the jumps from a region near the left boundary of A_1 (including A_1's left boundary), denoted as I_1, to a region near the right boundary of A_2, denoted as I_2. Setting $I_1 = [0.53, 0.59]$ and $I_2 = [0.7, 0.82]$, we investigate the maximum reactive current for any given $x \in I_1$: $g(x) := \max_{y \in I_2} J^+(x, y)$ for $x \in I_1$. The maximizer of this function g, whether it is equal to the value at the left boundary of A_1 or not, will determine which one of $\boldsymbol{\varphi}_1$ and $\boldsymbol{\varphi}_2$ is the A–B dominant transition path. By plotting the graph of the (rescaled) function g for several σ values around the critical value σ_1 in Fig. 9, we indeed find that it is the competition of two local maximizers of g that leads to the bifurcation of the dominant transition path from $\boldsymbol{\varphi}_2$ to $\boldsymbol{\varphi}_1$ as σ increasingly passes σ_1.

The bifurcation at the second critical value σ_2 of the noise amplitude σ is also due to the change in the MPCC and the dominant transition paths, via the competition of the local maximum in the interiors and the values at the boundary points of A_1 and A_2 for the function $J^+(x, y)$. The numerical evidences skipped.

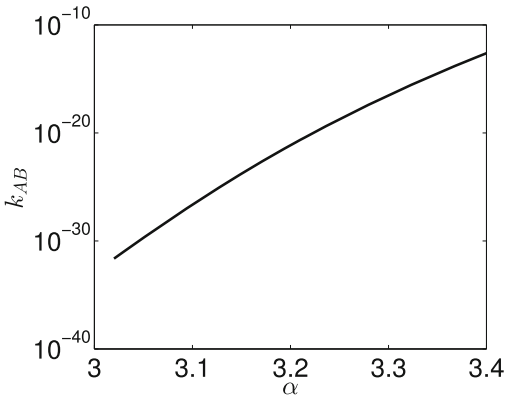

Fig. 10 κ_{AB} versus α

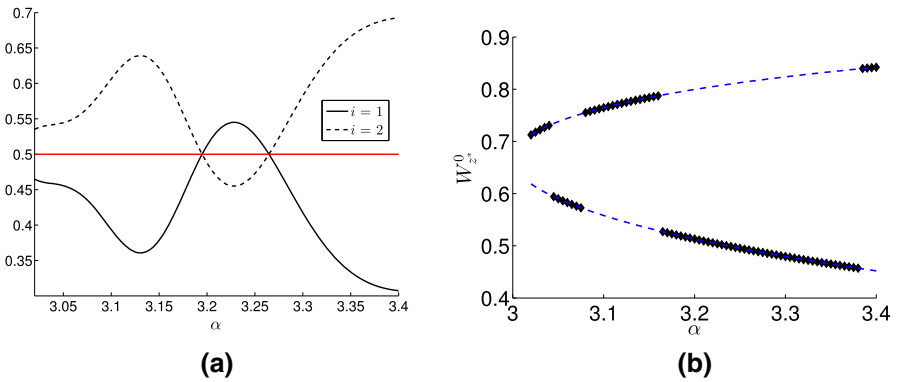

Fig. 11 The MPLP and the MCPP for $3.02 \leq \alpha \leq 3.40$. $\sigma = 0.02$, $\delta_a = \delta_b = 0.01$. The *horizontal straight line* in **a** indicates the threshold 0.5. The *dashed curves* in **b** represent the locations of the two periodic points for each α. **a** $r^-_{AB}(i)/(r^-_{AB}(1) + r^-_{AB}(2))$ versus α. **b** The MCPP

5.2.2 Change α

When $\alpha \in [3.02, 3.40]$, the only stable invariant set of the logistic map is the period-2 orbit. We are now interested in how the value of α influences the transition rate and the roles of the individual periodic points. Fix $\sigma = 0.02$ and $\delta_a = \delta_b = 0.01$. Figure 10 shows that the transition rate κ_{AB} increases in α and this dependency is nearly exponential. To identify the MPLP between the two periodic points ξ_1 and ξ_2 (ξ_1 is defined to be the smaller one), the probability mass $r^-_{AB}(i)/(r^-_{AB}(1)+r^-_{AB}(2))$ is plotted in Fig. 11a. As shown in this figure, ξ_1 is the MPLP only when α is approximately between 3.20 and 3.26. Figure 11b shows the MCPP in dark diamond-shaped dots for each α. For the range of α, we investigated here, there are four critical values of α where the MCPP switches between the two periodic points ξ_1 and ξ_2. As explained in Sect. 4.5, the MPLP and MCPP can be different in Fig. 11a, b.

6 Discussion

In conclusion, in order to study the stochastic instability of linearly stable periodic orbit from the perspective of noise-induced transitions, we have described the method based on the transition path theory and illustrated the example of the randomly perturbed logistic map. The introduced concepts of most-probable-last-passage point and the maximum competency point are novel descriptions of the stochastic instability for linearly stable periodic points. We demonstrated the capability of these two proposed perspectives to quantify the stochastic instabilities of the individual periodic point in one periodic orbit. It should be noted that although only the case of period-2 was analyzed here, our method can also be applied to other types of set A with more complex structures. In fact, our approach based on the transition path theory is generic to any ergodic stochastic dynamical systems, such as the multiplicative random perturbations, and to the arbitrary nonintersecting closed subsets A and B, such as the stable limit cycles in continuous-time dynamical systems.

References

Ahuja, R.K., Magnanti, T.L., Orlin, J.B.: Network Flows: Theory, Algorithms, and Applications. Prentice-Hall Inc, Upper Saddle River, NJ (1993)

Billings, L., Bollt, E.M., Schwartz, I.B.: Phase-space transport of stochastic chaos in population dynamics of virus spread. Phys. Rev. Lett. **88**, 234101 (2002)

Bollt, E.M., Billings, L., Schwartz, I.B.: A manifold independent approach to understanding transport in stochastic dynamical systems. Phys. D **173**(34), 153–177 (2002)

Cameron, M., Vanden-Eijnden, E.: Flows in complex networks: theory, algorithms, and application to Lennard–Jones cluster rearrangement. J. Stat. Phys. **156**(3), 427–454 (2014)

Dykman, M., McClintock, P., Smelyanski, V., Stein, N., Stocks, N.: Optimal paths and the prehistory problem for large fluctuations in noise-driven system. Phys. Rev. Lett. **68**(18), 2718 (1992)

E, W., Ren, W., Vanden-Eijnden, E.: Minimum action method for the study of rare events. Comm. Pure Appl. Math. **57**, 637–656 (2004)

E, W., Vanden-Eijnden, E.: Towards a theory of transition paths. J. Stat. Phys **123**(3), 503–523 (2006)

E, W., Vanden-Eijnden, E.: Transition-path theory and path-finding algorithms for the study of rare events. Annu. Rev. Phys. Chem. **61**, 391–420 (2010)

E, W., Zhou, X., Cheng, X.: Subcritical bifurcation in spatially extended systems. Nonlinearity **25**, 761 (2012)

Eyring, H.: The activated complex and the absolute rate of chemical reactions. Chem. Rev. **17**, 65–77 (1935)

Freidlin, M.I., Wentzell, A.D.: Random Perturbations of Dynamical Systems, 2 ed. Grundlehren der mathematischen Wissenschaften, New York: Springer (1998)

Graham, R., Hamm, A., Tél, T.: Nonequilibrium potentials for dynamical systems with fractal attractors or repellers. Phys. Rev. Lett. **66**(24), 3089–3092 (1991)

Heymann, M., Vanden-Eijnden, E.: The geometric minimum action method: a least action principle on the space of curves. Commun. Pure Appl. Math. **61**, 1052–1117 (2008)

Karmers, H.A.: Brownian motion in a field of force and the diffusion model of chemical reactions. Physica **7**, 284–304 (1940)

Kautz, R.L.: Activation energy for thermally induced escape from a basin of attraction. Phys. Rev. A **125**, 315–319 (1987)

Kautz, R.L.: Thermally induced escape: the principle of minimum available noise energy. Phys. Rev. A **38**(4), 2066–2080 (1988)

Kraut, S., Feudel, U.: Enhancement of noise-induced escape through the existence of a chaotic saddle. Phys. Rev. E **67**(1), 015204 (2003)

Luchinsky, D.G., Khonanov, I.A.: Fluctuation-induced escape from the basin of attraction of a quasiattractor. JETP Lett. **69**(11), 825–830 (1999)

Lu, J., Nolen, J.: Reactive trajectories and the transition path process. Probab. Theory Relat. Fields **161**(1–2), 195–244 (2015)

Maier, R.S., Stein, D.L.: Transition-rate theory for nongradient drift fields. Phys. Rev. E **69**(26), 3691 (1992)

Maier, R.S., Stein, D.L.: Escape problem for irreversible systems. Phys. Rev. E **48**(2), 931–938 (1993)

Matkowsky, B.J., Schuss, Z., Tier, C.: Diffusion across characteristic boundaries with critical points. SIAM J. Appl. Math. **43**(4), 673 (1983)

Matkowsky, B.J., Schuss, Z.: Diffusion across characteristic boundaries. SIAM J. Appl. Math. **42**(4), 822 (1982)

Metzner, P., Schütte, C., Vanden-Eijnden, E.: Transition path theory for Markov jump processes. Multiscale Model. Simul. **7**, 11921219 (2009)

Naeh, T., Klosek, M.M., Matkowsky, B.J., Schuss, Z.: A direct approach to the exit problem. SIAM J. Appl. Math. **50**(2), 595–627 (1990)

Noé, F., Schütte, C., Vanden-Eijnden, E., Reich, L., Weikl, T.R.: Constructing the equilibrium ensemble of folding pathways from short off-equilibrium simulations. Proc. Natl. Acad. Sci. USA **106**(45), 1901119016 (2009)

Ott, E.: Chaos in Dynamical Systems. Cambridge University Press, Cambridge (1993)

Silchenko, A.N., Beri, S., Luchinsky, D.G., McClintock, P.V.E.: Fluctuational transitions through a fractal basin boundary. Phys. Rev. Lett. **91**(17), 174104 (2003)

Silchenko, A.N., Beri, S., Luchinsky, D.G., McClintock, P.V.E.: Fluctuational transitions across different kinds of fractal basin boundaries. Phys. Rev. E **71**(4), 046203 (2005)

van Kampen, N.G.: Stochastic Processes in Physics and Chemistry, vol. 1, 2nd edn. North Holland, Amsterdam (1992)

Vanden-Eijnden, E.: Transition path theory. In: Ferrario, M., Ciccotti, G., Binder, K. (eds.) Computer Simulations in Condensed Matter Systems: From Materials to Chemical Biology, pp. 453–493. Springer, Berlin (2006)

Wan, X., Zhou, X., E, W.: Study of noise-induced transition and the exploration of the configuration space for the Kuromoto-Sivachinsky equation using the minimum action method. Nonlinearity **23**(3), 475–493 (2010)

Zhou, X., Ren, W., E, W.: Adaptive minimum action method for the study of rare events. J. Chem. Phys. **128**(10), 104111 (2008)

Zhou, X., E, W.: Study of noise-induced transitions in the Lorenz system using the minimum action method. Commun. Math. Sci. **7**, 341–355 (2009)